Pergamon

Int. J. Solids Structures Vol. 33, No. 23, pp. 3439–3462, 1996

0020-7683/96 $15.00 + .00

0020-7683(95)00184-0

SELF HEATING AND THERMAL FAILURE OF POLYMERS SUSTAINING A COMPRESSIVE CYCLIC LOADING

A. MOLINARI
LPMM, URA CNRS 1215, Université de Metz, Ile du Saulcy, 57045 Metz Cedex, France

and

Y. GERMAIN
CERDATO, Elf Atochem, 27470 Serquigny, France

(*Received* 12 *January* 1995; *in revised form* 19 *July* 1995)

Abstract—Self heating of polymers sustaining a compressive cyclic loading is assessed by theoretical analyses and experimental measurements. Steady-state solutions are obtained in the case of isotropic linear viscoelastic temperature sensitive materials and negligible inertia effects. The conditions of thermal failure associated with the nonexistence of steady-state solutions are discussed. The stability of steady states is also analysed, and conditions of thermal runaway are obtained. The extent to which these theoretical analyses are in agreement with experimental results is evaluated. Copyright © 1996 Elsevier Science Ltd

1. INTRODUCTION

This paper is aimed at analysing the deformation induced self heating in a cylindrical specimen, made of a polymeric material sustaining a cyclic compressive loading. The distribution of temperature is calculated in closed form and conditions of melting by thermal runaway are discussed. We also develop experimental measurements, and assess the extent to which agreement with theoretical analyses has been attained.

The control of self heating is of considerable importance in structural applications where polymeric materials are widely used (for example, rigid polymers in structures under low frequency regime or elastomers in vibration filters). This is particularly important for thermoplastics that have a very high temperature sensitivity and that can melt up to a certain temperature. For instance, thermoplastic elastomers (TPE) are new materials that can challenge traditional rubbers in many cases, providing that the workpiece can be properly designed to avoid catastrophic self heating. In addition, they offer a better ability in processing.

Basic experimental works devoted to the analysis of thermal failure of polymers can be found in Constable *et al.* (1970), Hertzberg (1976), Ratner and Korobov (1965), Riddell *et al.* (1966) and Takahara *et al.* (1980, 1981). Constable *et al.* (1970) and Takahara *et al.* (1980, 1981) also provided theoretical analyses where some simplifying assumptions were made. Assuming the uniformity of the temperature field, they calculated the steady-state temperature, but they did not consider the stability of that steady-state solution.

Catastrophic failure due to self heating is a common phenomena in dissipative materials. Among such phenomena, adiabatic shear banding, or the formation of hot lines observed by Tresca (1878) in high speed metal forming, are typical examples. These adiabatic shear bands come from the growth of an unstable plastic flow (Culver, 1973; Clifton, 1978; Bai, 1982; Molinari, 1985; Molinari and Clifton, 1987) related to the heat dissipated during the process and the resulting thermal softening of the material.

The problem discussed in this paper is quite different from the former problem where a viscoplastic temperature sensitive material was considered that sustained large monotonic deformations. However, an interesting analogy will be drawn from the discussion of the

existence and stability of the steady states resulting from the balance of the heat generated by the deformation process with the heat flux to the surroundings.

In this paper, we analyse the existence and stability of steady-state distributions of temperature and deformation in a cylinder made of a linear thermal sensitive viscoelastic material sustaining a compressive cyclic loading.

The organization is as follows. In Section 2 we describe the governing equations of the quasi-static problem, and introduce the viscoelastic constitutive law for a thermal sensitive isotropic, incompressible material. Two types of boundary conditions are prescribed in which the amplitude of the axial force or the amplitude of the axial displacement are controlled.

The equations governing the steady-state solutions are given in Section 3 in terms of the storage and loss moduli. The steady-state profiles of the temperature and deformation fields are obtained analytically in Section 4 for a thermorheologically simple material, under the assumption that the storage and loss moduli depend linearly on the temperature. The effects of the loading parameters and of the geometry of the specimen on the steady-state solutions are discussed.

The conditions of nonexistence of a steady-state solution are established. A material failure by thermal runaway necessarily appears in these cases.

A different case of thermal runaway, associated to the growth of any perturbation from an *unstable* steady-state solution, is also analysed. This case is studied in Section 5 with a simplified linearized stability analysis.

Finally, laboratory experiments are presented and discussed with respect to the theoretical analyses in the Section 6.

2. GOVERNING EQUATIONS

A cylindrical specimen (radius R, length h, Fig. 1) of a linear isotropic incompressible viscoelastic material is submitted to an axial cyclic loading. Note that the conditions of isotropy and incompressibility are well satisfied by elastomers. Small deformations are considered. Thermal expansion is neglected, but this point will be discussed later in Appendix A (see also Section 3).

Considering the decomposition of the Cauchy stress:

$$\sigma_{ij} = -p\delta_{ij} + s_{ij} \tag{1}$$

where p is the hydrostatic pressure and s_{ij} the deviatoric stress, the linear isotropic viscoelastic incompressible behavior is specified by the following Boltzmann law:

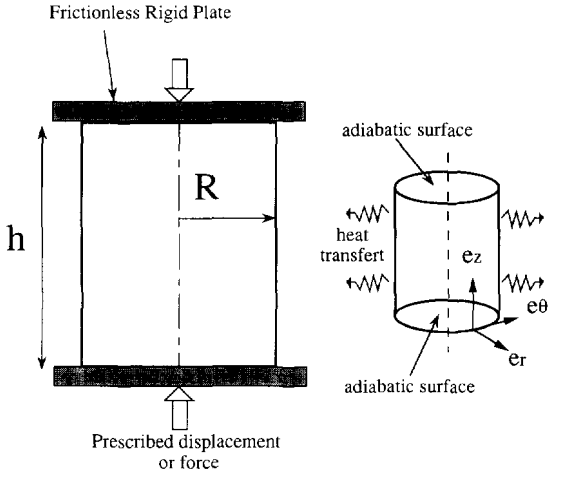

Fig. 1. Geometry of the specimen, and description of the mechanical and thermal boundary conditions.

$$s_{ij}(t) = 2\int_{-\infty}^{t} G(t-t', T)\dot{\varepsilon}_{ij}(t')\,dt' = 2G(\infty, T)\varepsilon_{ij}(t) + 2\int_{-\infty}^{t} [G(t-t', T) - G(\infty, T)]\dot{\varepsilon}_{ij}(t')\,dt' \tag{2}$$

where $G(\infty, T)$ is the equilibrium modulus at temperature T.

Thermal effects are included in the temperature dependence of the relaxation function G. $\dot{\varepsilon}_{ij}$ designates the strain rate; in the small deformation theory considered here $\dot{\varepsilon}_{ij}$ is the time derivative (in the distribution sense) of the infinitesimal strain tensor.

Incompressibility reads:

$$\dot{\varepsilon}_{ii} = 0 \tag{3}$$

where the convention of summation on the repeated indice is adopted.

The law (2), which relies on the Boltzmann's superposition principle, assumes that the absolute temperature T is time independent.

An important point of this paper is to analyse the steady state resulting from the balance in the heat generated by the dissipation of part of the mechanical work and the heat loss to the surroundings. The temperature is then time independent and the law (2) can be used. Small deviations with respect to this steady state (variations of temperature inducing small variations of G) will be occasionally considered.

The evolution of the temperature T is governed by the heat equation:

$$\rho c\frac{\partial T}{\partial t} - k\Delta T = \dot{Q} \tag{4}$$

where ρ is the volumic mass, c the specific heat capacity, k the heat conductivity, ΔT the Laplacian of the temperature and $\dot{Q}$ is the rate of calorific energy produced by the dissipation per unit volume.

Taking account of the cylindrical symmetry of the problem (geometry of the specimen and isotropy of the behavior) the equilibrium equations read in cylindrical coordinates:

$$\frac{\partial \sigma_{rr}}{\partial r} + \frac{\partial \sigma_{rz}}{\partial z} + \frac{\sigma_{rr} - \sigma_{\theta\theta}}{r} = 0,$$

$$\frac{\partial \sigma_{rz}}{\partial r} + \frac{\partial \sigma_{zz}}{\partial z} + \frac{\sigma_{rz}}{r} = 0. \tag{5}$$

The inertia effects are neglected. This point is discussed later.

Two types of *mechanical boundary conditions* will be considered.

2.1. *Prescribed axial displacement*

The axial component w of the displacement $\mathbf{u} = u\mathbf{e}_r + v\mathbf{e}_\theta + w\mathbf{e}_z$, see Fig. 1, is prescribed at the upper and lower faces of the cylinder. A periodic loading is superposed on a static compression $w_m < 0$:

$$w = w_m + w_0 \cos \omega t, \quad \text{at } z = h$$

$$w = 0, \quad \text{at } z = 0 \tag{6}$$

with $w_0 > 0$.

The extremities are frictionless

$$\sigma_{zr} = \sigma_{z\theta} = 0 \quad \text{at} \quad z = h \quad \text{and} \quad z = 0 \tag{7}$$

and the lateral surface is traction free.

2.2. *Prescribed axial force*

In some of the experiments presented later, an axial compressive force is prescribed and transmitted to the specimen by a rigid plate (Fig. 1) constrained to move vertically. The contact with the specimen is frictionless. The vertical displacement w is uniform at $z = h$, and equal to zero at $z = 0$. The amplitude of w is controlled by the prescribed force F:

$$F = F_m + F_0 \cos \omega t \quad (F_m < 0, F_0 > 0). \tag{8}$$

Inertia terms can be neglected in eqn (5) if the frequency ω is sufficiently small. An estimation of the range of admissible values of ω is obtained when considering, for sake of simplicity, the steady longitudinal oscillation of an elastic cylinder. It can be shown that the quasi-static hypothesis is justified when $\omega^2 \ll E/\rho h^2$, where E is the Young modulus. For a typical elastomer, with $E = 100$ MPa and $\rho = 1000$ kg m^{-3}, this condition reads:

$$\omega h \ll 316 \text{ m s}^{-1}.$$

The *thermal boundary conditions* specify the heat transfer at the lateral boundary:

$$k \frac{\partial T}{\partial r} + \lambda (T - T_0) = 0 \quad (\text{at } r = R) \tag{9}$$

where λ is a heat transfer coefficient, and T_0 is the external temperature. The extremities are assumed adiabatic.

3. STEADY-STATE SOLUTIONS

A cyclic axial prescribed displacement is now considered. The first step in the analysis consists in the determination of the steady state solutions. The stress and the strain fields are first calculated, by using an *a priori* form of the displacement field. The dissipated energy is then derived, and the temperature field is obtained by integration of the heat equation. The case of a prescribed axial stress is also discussed.

Thermal dilatation is not taken into account in the following analysis, but it is shown in Appendix A that the results are not affected by this effect.

3.1. *Strain and stress analysis*

Taking advantage of the symmetries of the problem, and of the fact that the extremities are adiabatic, the following forms of the displacement field (similar to the isothermal problem) and of the temperature field, are considered:

$$u(r, t) = u_0(r) \cos \omega t - \frac{w_m}{2} \frac{r}{h}$$

$$w(r, t) = \varepsilon_0 z \cos \omega t + w_m \frac{z}{h} \tag{10}$$

$$T = T(r, t) \tag{11}$$

where

$$\varepsilon_0 = \frac{w_0}{h} \tag{12}$$

is the amplitude of the prescribed sinusoidal deformation. The displacement boundary conditions are satisfied.

The strain tensor is given by:

$$\varepsilon_{rr} = \frac{\partial u}{\partial r}(r, t), \quad \varepsilon_{\theta\theta} = \frac{u(r, t)}{r}, \quad \varepsilon_{zz} = A(t)$$

$$\varepsilon_{ij} = 0 \quad \text{when } i \neq j \tag{13}$$

with

$$A(t) = \varepsilon_0 \cos \omega t + \frac{w_m}{h} \tag{14}$$

$u(r)$ can be obtained from the incompressibility condition (3):

$$\frac{\partial u}{\partial r} + \frac{u}{r} + A = 0. \tag{15}$$

It yields

$$u(r, t) = -\frac{A(t)}{2} r \quad \text{or} \quad u_0(r) = -\frac{\varepsilon_0 r}{2} \tag{16}$$

and

$$\varepsilon_{rr} = -\frac{A(t)}{2}, \quad \varepsilon_{\theta\theta} = -\frac{A(t)}{2}, \quad \varepsilon_{zz} = A(t). \tag{17}$$

The deviatoric stresses are obtained after substitution of eqn (17) in the constitutive law (2):

$$s_{zz} = 2G_\infty(T_m)A(t) + 2\int_{-\infty}^{t} [G(t-t', T_m) - G_\infty(T_m)]\dot{A}(t')\,dt',$$

$$s_{\theta\theta} = s_{rr} = -\frac{s_{zz}}{2}. \tag{18}$$

$G_\infty(T_m) = G(\infty, T_m)$ is the equilibrium modulus expressing the material response at temperature T_m to the static loading w_m, after an infinite time.

T_m is the mean temperature (i.e. time averaged), at the point considered, when the steady state is established. Actually the temperature oscillates around T_m during a cycle. Assuming that the amplitude of the temperature fluctuation is small enough (this is checked in Appendix B), it can be considered that:

$$G(t, T) \approx G(t, T_m). \tag{19}$$

Developing eqn (18) leads to:

$$s_{zz} = 2G_\infty(T_m)\frac{w_m}{2} + 2\varepsilon_0[G'(\omega, T_m)\cos \omega t - G''(\omega, T_m)\sin \omega t],$$

$$s_{\theta\theta} = s_{rr} = -\frac{s_{zz}}{2}, \tag{20}$$

with the storage modulus G' and the loss modulus G'' defined by (Christensen, 1971):

$$G'(\omega, T_m) = G_\infty(T_m) + \omega \int_0^\infty [G(u, T_m) - G_\infty(T_m)] \sin(\omega u)\, du,$$

$$G''(\omega, T_m) = \omega \int_0^\infty [G(u, T_m) - G_\infty(T_m)] \cos(\omega u)\, du. \tag{21}$$

It can be noted that the spatial dependence of s_{zz} appears through the r-dependence of T_m.

From the second equilibrium eqn (5) where $\sigma_{rz} = 0$, it results that the pressure p (and consequently σ_{ij}) is solely r-dependent. Furthermore, as indicated by the first eqn (5), σ_{rr} is constant in the cylinder, and actually equal to zero, since the lateral boundary is traction free. Thus:

$$p(r, t) = s_{rr}(r, t). \tag{22}$$

As soon as the temperature field T_m is determined, the deviatoric stresses and the pressure are obtained with eqns (20) and (22), and the stresses are:

$$\sigma_{zz} = -p + s_{zz} = \tfrac{3}{2} s_{zz},$$
$$\sigma_{rr} = \sigma_{\theta\theta} = 0. \tag{23}$$

3.2. *Thermal analysis*

Time averaging of the heat eqn (4) over a cycle leads to the following result:

$$-k \frac{1}{r} \frac{d}{dr}\left(r \frac{dT_m}{dr}\right) = \frac{\omega}{2\pi} \Delta Q \tag{24}$$

where the mean temperature is defined by:

$$T_m(r) = \frac{\omega}{2\pi} \int_{\text{cycle}} T(r, t)\, dt. \tag{25}$$

The dissipated energy per unit volume and per cycle ΔQ, is equal to the area of the hysteresis loop:

$$\Delta Q = \int_{\text{cycle}} \sigma_{ij}(t) \dot{\varepsilon}_{ij}(t)\, dt = \int_{\text{cycle}} \tfrac{3}{2} s_{zz}(t) \dot{\varepsilon}_{zz}(t)\, dt = 3\pi \varepsilon_0^2 G''(\omega, T_m) \tag{26}$$

according to eqns (14), (17) and (20).

Finally T_m is the solution of the following equation:

$$-\frac{k}{r} \frac{d}{dr}\left(r \frac{dT_m}{dr}\right) = \tfrac{3}{2} \omega \varepsilon_0^2 G''[\omega, T_m(r)] \tag{27}$$

which can be integrated when G'' is known. The boundary condition

$$k \frac{dT_m}{dr} + \lambda (T_m - T_0) = 0, \quad \text{for } r = R \tag{28}$$

comes from eqn (9) after time averaging.

3.3. *Resulting axial force*

The axial force F is obtained after substitution of the stress given by eqns (20) and (23) in:

$$F = \int_0^R \sigma_{zz} 2\pi r \, dr = \int_0^R \tfrac{3}{2} s_{zz} 2\pi r \, dr \tag{29}$$

leading to:

$$F = F_m + F_1 \cos \omega t - F_2 \sin \omega t \tag{30}$$

where the components of the dynamical response are:

$$F_1 = 6\pi\varepsilon_o \int_0^R rG'[\omega, T_m(r)] \, dr,$$

$$F_2 = 6\pi\varepsilon_o \int_0^R rG''[\omega, T_m(r)] \, dr. \tag{31}$$

The static force associated to the constant displacement w_m is:

$$F_m = 6\pi \frac{w_m}{h} \int_0^R rG_x[T_m(r)] \, dr. \tag{32}$$

The phase angle ψ, between the applied displacement and the resulting force, due to dissipative effects, appears when eqn (30) is rewritten in the form:

$$F = F_m + F_o \cos(\omega t + \psi) \tag{33}$$

with

$$F_o = \sqrt{F_1^2 + F_2^2} \tag{34}$$

$$\tan \psi = \frac{F_2}{F_1}. \tag{35}$$

For an uniform temperature field, the loss tangent reduces to the classical expression

$$\tan \psi = \frac{G''(\omega, T)}{G'(\omega, T)}.$$

3.4. *Prescribed axial force*

The boundary condition, eqn (8), is considered now. In that case the amplitude w_o of the displacement is a function of the prescribed amplitude F_o of the axial force. This relation, given by eqns (34) and (31), is highly nonlinear in the nonisothermal problem, since the dependence of T_m with respect to $\varepsilon_o = w_o/h$ is ruled by the differential eqn (27). For a given F_o, it will be shown later that a nonunique solution for w_o is possible.

The relation between F_o and w_o can be simplified, as generally done in the literature, when the uniformity of the temperature field can be considered as a reasonable assumption. Then T_m and $\varepsilon_o = w_o/h$ are solutions of eqns (C5) and (C6) of Appendix C. For a stubby specimen, the assumption of uniform temperature is too crude, and the full solution is necessary.

4. ANALYSIS OF SELF HEATING AND THERMAL FAILURE

An important point of the paper is to determine the conditions under which self heating leads to the destruction of the specimen. For thermoplastics this catastrophic process is a consequence of the melting of the material.

For the purpose of designing structural components, it is useful to understand in a systematic analysis, the effects of the material parameters, as well as the effects of the geometrical and loading parameters. A special attention will be devoted to a particular thermoplastic elastomer, a PEBAX (shore D hardness of 40) provided by Elf Atochem. The PEBAX is a block copolymer made of polyamid and polyether segments. The amorphous polyether phase is cross linked by the semi-crystalline polyamid. The melting temperature of the PEBAX is 441 K.

Variation of the material properties will be also considered for illustration purpose.

4.1. *Material properties*

The viscoelastic properties are characterized by the moduli $G'(\omega, T)$, $G''(\omega, T)$. Typical experimental data for the PEBAX elastomer are reported in Fig. 2. The variations of G' and G'' are presented in terms of the reduced temperature $T_{red} = T-(1/\beta)\ln(\omega/\omega_0)$, where β and ω_0 are material characteristics. The tests are conducted for different frequencies ($\omega/2\pi = 1, 10, 100\ s^{-1}$) and various temperatures. Since it is apparent that all the results can be represented on a single curve [the master curve, Ferry (1980)], the material considered is thermorheologically simple in the range of parameters considered in this paper.

It appears also that G' and G'' can be approximated, for that material, by piecewise linear functions of the reduced variable:

$$G'(\omega, T) = h_1 - h_2\left(T - \frac{1}{\beta}\ln\frac{\omega}{\omega_0}\right) \tag{36}$$

$$G''(\omega, T) = g_1 - g_2\left(T - \frac{1}{\beta}\ln\frac{\omega}{\omega_0}\right) \tag{37}$$

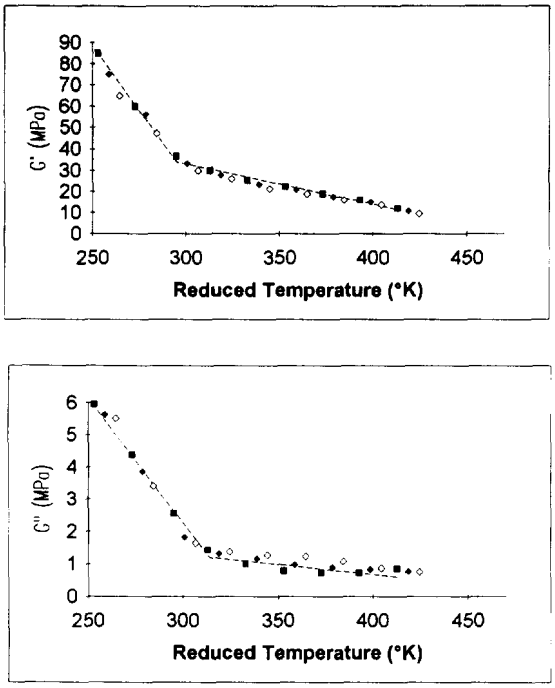

Fig. 2. Variations of the storage and of the loss moduli G' and G'' of the PEBAX elastomer, in terms of the reduced temperature $T_{red} = T-(1/\beta)\ln(\omega/\omega_0)$. The experimental data correspond to different values of ω ($\diamond$ $\omega/2\pi = 1\ s^{-1}$, $\blacklozenge$ $\omega/2\pi = 10\ s^{-1}$, $\blacksquare$ $\omega/2\pi = 100\ s^{-1}$). The dashed lines represent the fit of these data by using eqns (36) and (37) of G' and G'' and the parameters given in Table 1.

Table 1

	PEBAX
ω_o	628 rad s^{-1}
β	0.4 K^{-1}
k	0.2 W m^{-1}K^{-1}
λ	20 W m^{-2}K^{-1}
ρc	2×10^6 J K^{-1}m^{-3}

	PEBAX	
	$T_{red} \leqslant 295$ K	$T_{red} \geqslant 295$ K
h_1	390 MPa	91 MPa
h_2	1.2 MPa K^{-1}	0.193 MPa K^{-1}
	$T_{red} \leqslant 314$ K	$T_{red} \geqslant 314$ K
g_1	25.3 MPa	3.1 MPa
g_2	0.077 MPa K^{-1}	0.006 MPa K^{-1}

where the parameters h_1, h_2, g_1, g_2 are constant on certain temperature intervals. The material (mechanical and thermal) parameters for the PEBAX are presented in Table 1. The fit of experimental measurements obtained by using these data can be appreciated in Fig. 2. The changes in the slopes near $T_{red} = 300$ K can be attributed to a melting of the polyether phase.

4.2. *Analytical solution*

The case where G' and G'' have a linear T-dependence, as given by eqns (36) and (37) (with h_1, h_2, g_1, g_2 constant), constitutes a basic problem to be solved.

The temperature T_m is solution of eqn (27). Using the expression (37) of G'', it yields:

$$\frac{d^2T_m}{dr^2} + \frac{1}{r}\frac{dT_m}{dr} - a^2T_m = -b^2 \tag{38}$$

with:

$$a^2 = \frac{3}{2}\frac{\omega}{k}\varepsilon_o^2 g_2, \quad b^2 = a^2\left[\frac{g_1}{g_2} + \frac{1}{\beta}\ln\left(\frac{\omega}{\omega_o}\right)\right]. \tag{39}$$

Note that these terms are positive according to the following conditions for the material properties:

$$g_2 \geqslant 0, \quad G''(\omega, 0) \geqslant 0.$$

The general solution of eqn (38) involves the modified Bessel functions $I_o(ar)$ and $K_o(ar)$. Since $K_o(ar)$ is singular at $r = 0$, it does not appear in the result. Taking account of the boundary condition (28), the solution reads:

$$T_m(r) = \frac{b^2}{a^2} + \alpha I_o(ar) \tag{40}$$

with

$$\alpha = -\lambda\left(\frac{b^2}{a^2} - T_0\right)[kaI_1(aR) + \lambda I_0(aR)]^{-1}. \tag{41}$$

The components of the axial force are obtained from eqn (31) with the expressions (36) and (37) of G' and G'':

$$F_1 = 3\pi\varepsilon_0 R^2\left[-2\alpha h_2 \frac{1}{aR} I_1(aR) + h_1 - h_2\frac{g_1}{g_2}\right],$$

$$F_2 = -6\pi\varepsilon_0 \alpha g_2 \frac{R}{a} I_1(aR). \tag{42}$$

The case where G'' does not depend on the temperature is of interest. It can be deduced from the general solution as the limiting case of g_2 vanishing to zero. Using the asymptotic expansion of the modified Bessel functions for small arguments, the following results are derived:

$$T_m(r) = T_0 + \frac{3}{8}\frac{\omega}{k}\varepsilon_0^2 G''(\omega)\left(R^2 - r^2 + 2R\frac{k}{\lambda}\right) \tag{43}$$

$$F_1 = 3\pi\varepsilon_0 R^2\left[h_1 - h_2 T_0 + h_2\frac{\ln\omega}{\beta} - \tfrac{3}{4}h_2\frac{R}{k}\varepsilon_0^2\omega G''(\omega)\left(\frac{k}{\lambda} + \frac{R}{4}\right)\right],$$

$$F_2 = 3\pi\varepsilon_0 R^2 G''(\omega). \tag{44}$$

These results are easily obtained by direct integration of eqns (27) and (31), which is particularly simple when G'' is temperature independent.

The analytical solution (40)–(42) can be used to analyse experiments as far as G' and G'' can be represented by a linear relation with respect to T as given by eqns (36) and (37). A checking of the extremal values of the temperature in the specimen, consistent with the G' and G'' data used, is necessary *a posteriori*.

4.3. *Parametrical analysis and discussion*

The results corresponding to a PEBAX elastomer are now discussed. The material data are found in Table 1. The external temperature T_0 is kept equal to 320 K, unless otherwise specified. Due to the condition that $T \geqslant 320$ K in the specimen, it is seen in Fig. 2 and Table 1, that G' and G'' can be represented by linear functions with respect to the reduced variable $T - (1/\beta)\ln(\omega/\omega_0)$. Indeed, for the values of the temperature and of ω considered here, the parameters h_1, h_2, g_1, g_2 are constants given in the column on the right of Table 1. Cases where these parameters are piecewise constant will be addressed later.

4.3.1. *Effects of loading parameters.* We consider a cylinder with a radius R of 10^{-2}m.

The evolution of the amplitude F_0 of the axial force with respect to the amplitude of the deformation ε_0, for $\omega = 100\ s^{-1}$ is represented in Fig. 3. The dashed line corresponds to the isothermal linear viscoelastic behavior ($T = T_0$ in the specimen). If the thermal effects are accounted for, a maximum F_{0c} of the bearing capacity is found at the deformation ε_{0c}. The deviation with respect to the dashed line manifests the increasing importance of self heating and thermal softening, due to the larger input of energy produced when ε_0 is increased. The importance of thermal effects is illustrated by the temperature rise at the center of the specimen represented in Fig. 4.

Looking again at Fig. 3, it is found that no stationary solution exists for an applied force larger than $F_{0c} = 651$N. In that case the rate of dissipation is larger than the external heat losses. No equilibrium state can be reached. The transient response leads to an unbounded rise of temperature.

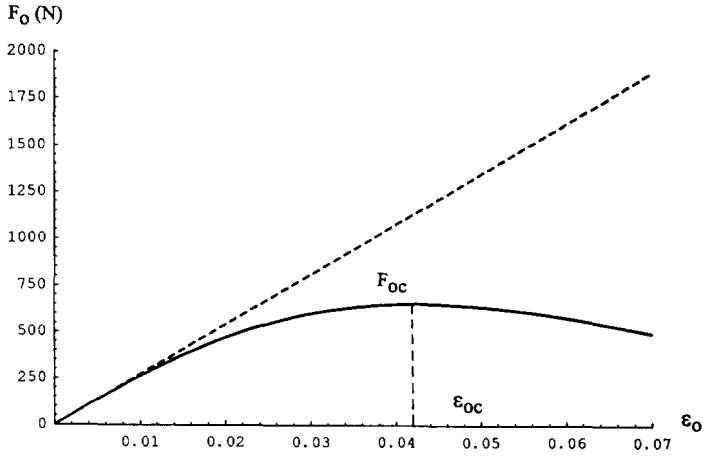

Fig. 3. Evolution of the amplitude F_0 of the axial force in terms of the amplitude ε_0 of the axial strain for $\omega = 100\ s^{-1}$ and $T_0 = 320$ K. Note that F_0 presents a maximum when thermal effects are accounted for (continuous line), while F_0 increases in the isothermal problem (dashed line). For $\varepsilon_0 \geqslant 0.07$ the melting conditions are attained.

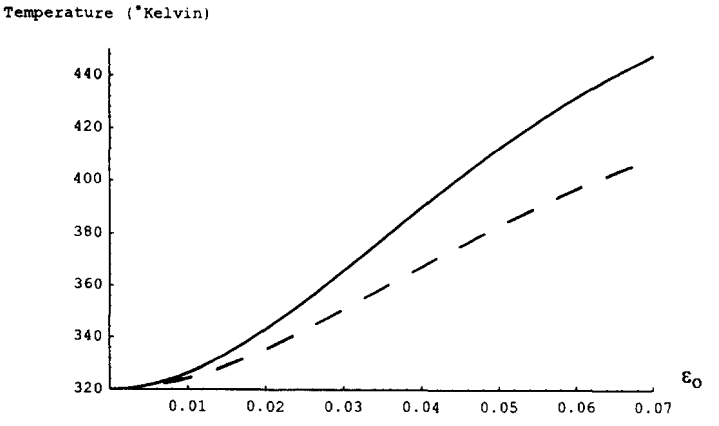

Fig. 4. Temperature at the center (——) and at the lateral boundary (---) with respect to the amplitude of the axial deformation (for $\omega = 100\ s^{-1}$).

For $F \leqslant F_{oc}$, one or two stationary states are associated with the same level of force, when keeping the temperature under the melting point. Even when two solutions are found, it does not mean that they have a physical existence, since they can be unstable. The problem of stability will be discussed in Section 5.

For a prescribed deformation ε_0, there exists only one single steady state until the melting point is reached.

An interesting comparison can be made with the analysis of the existence of steady states in the simple shearing of thermo–viscoplastic materials. Leroy and Molinari (1992) have given an extended account of the literature on that subject. They consider a layer of a nonNewtonian temperature-sensitive fluid sustaining a constant velocity on the boundaries, or a constant shear stress, or a linear combination of stress and velocity. For some material behaviors (exponential temperature dependence, for example), the analysis of steady states shows a variation of the shear stress with respect to the velocity on the boundary similar to the evolution, represented in Fig. 3, of the force F_0 with respect to the amplitude ε_0 of the cyclic deformation. In both problems a thermal runaway occurs when the prescribed force is large enough. This analogy comes from the fact that in both cases the steady states are the result of the balance between the heat produced by dissipation and the heat removal to the surroundings.

A further analogy will appear in the analysis of the stability of the steady states in the next paragraph.

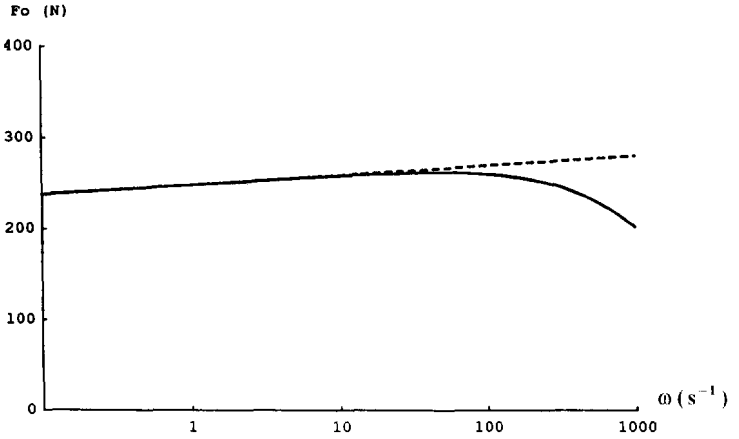

Fig. 5. Evolution of the amplitude F_0 of the axial force, in terms of ω (logarithmic scale), for a value of the amplitude of the deformation of $\varepsilon_0 = 0.01$ and for $T_0 = 320$ K. Note again the existence of a maximum for F_0 when the thermal effects are accounted for (continuous line) while F_0 increases continuously in the isothermal case (dashed line).

In Fig. 5, where the amplitude of the deformation is kept at the constant value of $\varepsilon_0 = 0.01$, the evolution of F_0 in terms of ω is considered. The curve corresponding to the ideally isothermal problem ($T = T_0$) is continuously increasing, since G' increases with ω. The second curve with a maximum F_{0c} at ω_c takes account of the thermal softening effects. At high frequencies, these effects overcome the viscoelastic stiffening, since then the heat is less easily evacuated to the surroundings. For larger values of ε_0, the thermal effects are magnified. This results in a decrease of ω_c as illustrated by Fig. 6(a). A similar conclusion is drawn from Fig. 6(b) where increasing values of ω are considered.

4.3.2. *Effect of geometry*. To analyse the effect of the radius R of the specimen, the mean value of the axial stress $F_0/\pi R^2$ is plotted as a function of ε_0, for $\omega = 100\ s^{-1}$, and different values of R, Fig. 7. For increasing values of the radius, the maximum force F_{0c} and the deformation ε_{0c} at which this force is attained, decrease. This results from the higher temperature attained at the center of the specimen having the larger radius, as a consequence of the larger time for the heat to diffuse from the center to the lateral boundary.

The effects of the thermal transfer coefficients k and λ are illustrated in the Fig. 8 for $R = 0.015$ m. Decreasing the values of k or λ leads to a similar effect as increasing the radius, since in both cases the time for heat transfer is increased. The relative importance of the parameters k, λ and R is well illustrated by the results of eqns (43) and (44), albeit restricted to the case where G'' does not depend on T. It is easily recognized that the contributions of diffusion and of heat transfert at the boundary can be expressed in terms of the ratios k/R^2 and λ/R.

4.3.3. *Case of piecewise linear functions* G′ *and* G″. The preceding calculations were made under conditions where G' and G'' could be represented by linear functions with respect to the reduced variable $T-(1/\beta)\ln(\omega/\omega_0)$, of the form of eqns (36) and (37).

In this subsection, we consider conditions where the range of temperature is such that G' and G'' cannot be considered as linear functions of the reduced variable but rather as piecewise linear functions of that variable. An illustration is provided by a cylinder of PEBAX elastomer of radius $R = 10^{-2}$m, sustaining a cyclic compressive loading under an external temperature of $T_0 = 253$ K. The evolution of the amplitude F_0 of the axial force in terms of the amplitude ε_0 of the deformation is represented in Fig. 9 for $\omega = 100\ s^{-1}$. Two analytical branches S_1 and S_2 are easily obtained. S_1 (respectively, S_2) corresponds to the case where the reduced temperature in the specimen is everywhere less than 295 K (respectively, larger than 314 K), allowing the use of the constant values of h_1, h_2, g_1, g_2 given in the first (respectively, second) column of Table 1. The solution S_1 (respectively, S_2) refers to small (respectively, large) values of ε_0, see Fig. 9. They are represented by the continuous

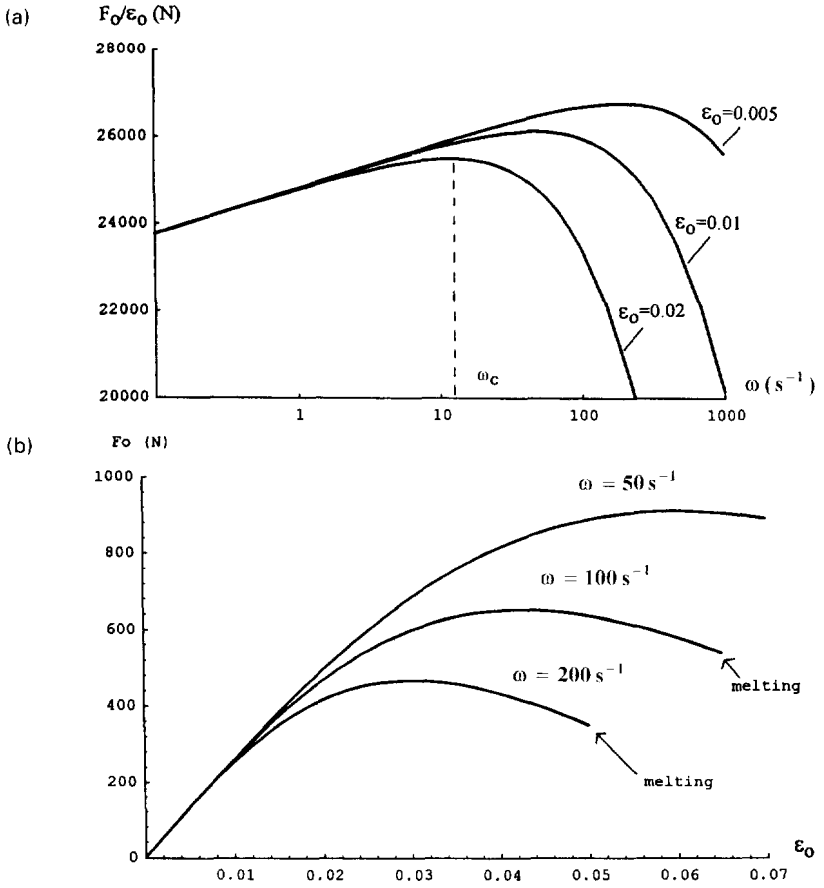

Fig. 6. (a) Amplification of the thermal effects with larger values of the amplitude of the deformation ε_0. Note that the maximum amplitude of the force F_{oc} and the corresponding frequency ω_c decrease when ε_0 increases. Note also that we have considered F_0/ε_0 in order to normalize the results. (b) Amplification of the thermal effects with larger values of the frequency ω.

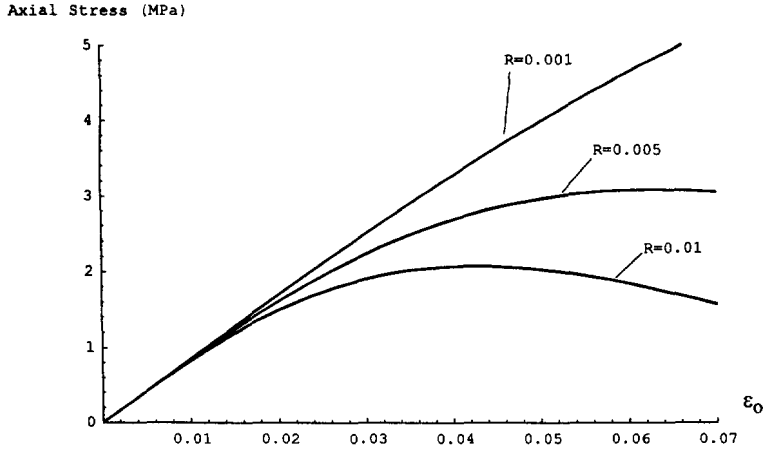

Fig. 7. Axial stress $F_0/\pi R^2$ in terms of ε_0 for $\omega = 100\ s^{-1}$. This figure illustrates the amplification of the thermal effects resulting in a reduction of the bearing load capacity for larger values of the radius R.

lines. The dashed lines indicate the cases where the analytical solution does not remain rigorous. This occurs when the increase of temperature in the bulk of the specimen leads to a violation of the conditions stated in the Table 1. Note that the maximum of the force F_0 is found on the branch S_2.

A finite element calculation was performed for sake of comparison. The stationary solution was calculated iteratively in the following way. The frequency ω is given. At the

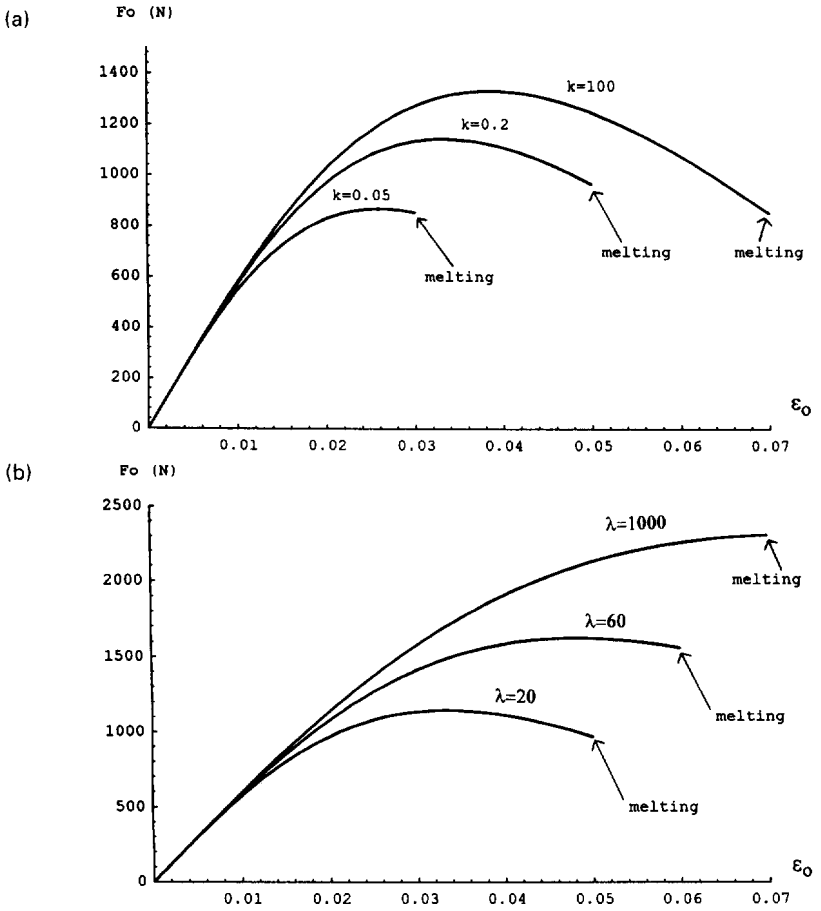

Fig. 8. Amplification of the thermal effects for decreasing values of: (a) the heat conductivity k (W $m^{-1}K^{-1}$); and (b) the thermal transfer coefficient at the boundary λ (W $m^{-2}K^{-1}$) ($R = 0.015$ m, $\omega = 100\ s^{-1}$).

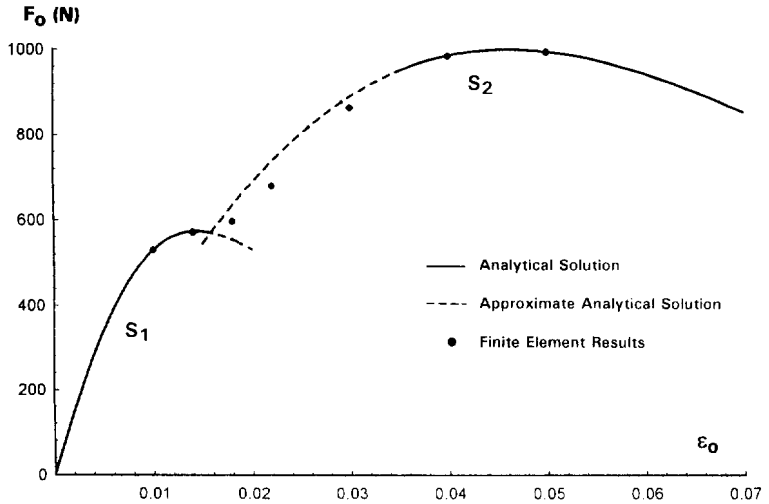

Fig. 9. Force F_o versus deformation ε_o for the PEBAX elastomer submitted to $\omega = 100\ s^{-1}$ at a value of the external temperature T_o of 253 K. The radius R has a value of 10 mm. Two analytical branches S_1 and S_2 are obtained (continuous and dashed line). Finite element results are compared with the analytical solutions.

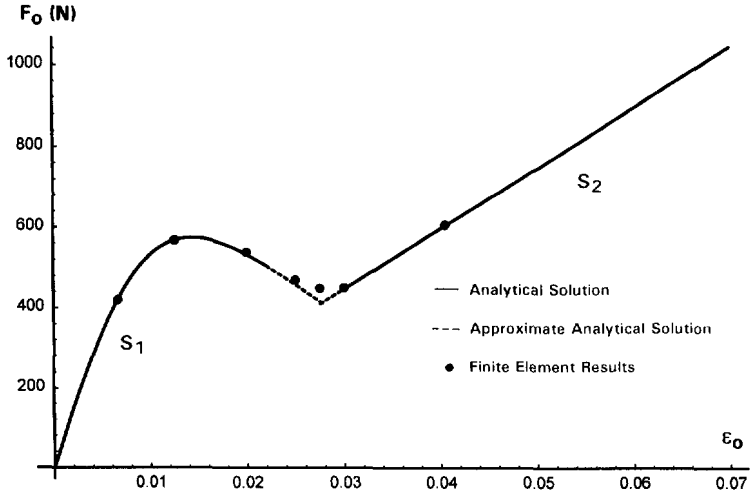

Fig. 10. Analytical solutions compared with finite element results for the model material described in Table 2 and for $\omega = 100\ s^{-1}$, $T_0 = 253$ K, $R = 10$ mm. Note that a local maximum in the force F_0 is obtained on the branch S_1.

Table 2

	$T_{red} \leqslant 310$ K	$T_{red} \geqslant 310$ K
h_1	390 MPa	15.75 MPa
h_2	1.2 MPa K^{-1}	0
g_1	25.3 MPa	1.5 MPa
g_2	0.077 MPa K^{-1}	0

nth step of the calculation the temperature field T_n is assumed to be known. The stress and strain fields $\underline{\underline{\sigma}}_n$ and $\underline{\underline{\varepsilon}}_n$ are obtained with the mechanical equations. The resulting heat production leads, after solving the energy equation, to a correction of the temperature field T_{n+1} that serves for the calculation at the $(n+1)$th step.

It is of interest to note in Fig. 9 that the finite element results exactly follow the analytical solutions (continuous line) and are also close to the approximate analytical solutions (dashed lines).

In other cases, a local maximum is found on the branch S_1 as illustrated for $\omega = 100\ s^{-1}$ and $T_0 = 253$ K in the Fig. 10, obtained for a model material whose characteristics are reported in Table 2. It is of note to remark that the linear growth of the solution S_2 is a consequence of G' and G'' being constant for $T_{red} \geqslant 310$ K. Here again the approximate analytical solution follows closely the results provided by the finite element calculations.

5. STABILITY ANALYSIS

The analysis has been restricted so far to the mathematical existence of steady-state solutions, but their physical existence, which is conditional to their stability, was not established. This section is aimed at analysing the influence of the loading conditions on the stability of the steady states.

5.1. *Simplified approach*

Significant stability results are obtained when some simplifying assumptions are made. We assume that the temperature field is uniform in the sample. This is realized in thin specimens. Any development of heterogeneity is disregarded. The analysis of tensile tests, where necking could appear, is not discussed.

Finally, the phenomena considered here are those where the characteristic time of growth of the instability is large with respect to the period of a cycle. This latter hypothesis

implies that the temperature depends on a fast time $t_0 = t$ (the physical time) and a slow time $t_1 = \varepsilon t$ where ε is a small parameter:

$$T = T(t_0, t_1). \tag{45}$$

The dependence on t_0 describes the temperature variation on a cycle, while the dependence on t_1 follows the development of the instability.

Since by assumption the solution is uniform, the energy equation takes on the following form [see eqn (C4) in Appendix C]:

$$\rho c \frac{\mathrm{d}T}{\mathrm{d}t}(t_0, t_1) + \kappa[T(t_0, t_1) - T_0] = \dot{Q} \tag{46}$$

where $\dot{Q}$ is the heat generation per unit volume and time. The heat transfer at the lateral boundary is characterized by the transfer coefficient:

$$\kappa = \frac{2\lambda}{R}. \tag{47}$$

The stability of the steady-state solutions is now analysed in the framework of the linearized stability analysis. A small perturbation is superimposed on the steady-state temperature profile. A linear evolution equation for that perturbation will be derived. The problem is then considered as linearly stable if the perturbation decays and linearly unstable if it grows. The analysis is restricted to weak instabilities having a characteristic growth time much larger than the period of a cycle. Then the relevant variable in the stability analysis can be taken as the time average of the temperature on a cycle, which is solely dependent on the slow time t_1:

$$\bar{T}(t_1) = \frac{\omega}{2\pi} \int_{t_0}^{t_0 + (2\pi/\omega)} T(t_0', t_1)\, \mathrm{d}t_0'. \tag{48}$$

The evolution equation for $\bar{T}$ can be obtained from eqn (46), by taking account of

$$\frac{\mathrm{d}}{\mathrm{d}t} T(t_0, t_1) = \frac{\mathrm{d}T}{\mathrm{d}t_0} + \varepsilon \frac{\mathrm{d}T}{\mathrm{d}t_1}$$

that, after averaging with respect to t_0 on a cycle, becomes:

$$\overline{\frac{\mathrm{d}T}{\mathrm{d}t}} = \varepsilon \overline{\frac{\mathrm{d}T}{\mathrm{d}t_1}} = \varepsilon \frac{\mathrm{d}\bar{T}}{\mathrm{d}t_1} = \frac{\mathrm{d}\bar{T}}{\mathrm{d}t}.$$

Finally we get:

$$\rho c \frac{\mathrm{d}\bar{T}}{\mathrm{d}t} + \kappa(\bar{T} - T_0) = \tfrac{3}{2}\omega \varepsilon_0 (\bar{T})^2 G''(\omega, \bar{T}). \tag{49}$$

The right-hand side comes from eqn (26) (multiplied by $\omega/2\pi$) where T_m is replaced by $\bar{T}$. This is consistent since $\bar{T}$ is slowly varying with respect to time, and can therefore be taken constant on a cycle (or on several cycles).

Considering now a steady-state solution, the time derivative can be canceled in eqn (49). The steady-state temperature T_m satisfies the equation:

$$\kappa(T_m - T_0) = \tfrac{3}{2}\omega\varepsilon_0(T_m)^2 G''(\omega, T_m). \tag{50}$$

Substracting eqns (49) and (50) results in the following differential equation that governs the stability of steady states:

$$\rho c\frac{d(\bar{T}-T_m)}{dt} + \kappa(\bar{T}-T_m) = \tfrac{3}{2}\omega[\varepsilon_0(\bar{T})^2 G''(\omega, \bar{T}) - \varepsilon_0(T_m)^2 G''(\omega, T_m)]. \tag{51}$$

During the initial stage of the development of instability, $\bar{T}$ remains close to T_m. Therefore it was justified to use the constitutive law (2) based on the Boltzmann principle, from which eqn (49) was obtained.

After linearization of eqn (51), a first-order linear differential equation governing the evolution of $\bar{T} - T_m$ is obtained. The stability condition reads:

$$\Lambda < 0 \tag{52}$$

with

$$\Lambda = \tfrac{3}{2}\omega\left[2\frac{d\varepsilon_0}{dT}(T_m)\varepsilon_0(T_m)G''(\omega, T_m) + \varepsilon_0(T_m)^2\frac{d}{dT}G''(\omega, T_m)\right] - \kappa. \tag{53}$$

For a *prescribed cyclic displacement*, we have $\dfrac{d\varepsilon_0}{dT} = 0$, and eqn (53) reduces to:

$$\Lambda = \tfrac{3}{2}\omega\varepsilon_0^2\frac{dG''}{dT} - \kappa. \tag{54}$$

This quantity is negative when $dG''/dT \leqslant 0$. It follows that the steady states associated to a prescribed cyclic displacement on the PEBAX elastomer are stable for the range of temperature where G'' is decreasing. Note that there exist viscoelastic materials for which dG''/dT can be positive. For these materials, instability of steady states is not excluded in the case of a prescribed cyclic displacement.

For a *prescribed amplitude of the cyclic force* F_0, ε_0 (T_m) is given by eqn (C6) of Appendix C:

$$\varepsilon_0(T_m) = \frac{F_0}{3\pi R^2}[G'(\omega, T_m)^2 + G''(\omega, T_m)^2]^{-1/2}. \tag{55}$$

The stability condition (52) reads now:

$$\Lambda = \tfrac{3}{2}\omega\left[\frac{F_0}{3\pi R^2(G'^2 + G''^2)}\right]^2\left[-2G''G'\frac{dG'}{dT} + (G'^2 - G''^2)\frac{dG''}{dT}\right] - \kappa < 0. \tag{56}$$

It can be checked that the marginal stability condition $\Lambda = 0$ corresponds to the steady state at the maximum of the curve F_0 versus ε_0 represented in Figs 3 or 11. The steady states on the left of the maximum are stable (subcritical branch), while those on the right are unstable (supercritical branch). It can be shown that the signs of dF_0/dT_m and $-\Lambda$ are identical, and that $dT_m/d\varepsilon_0 > 0$.

The steady states represented in the Fig. 11 are obtained for the PEBAX elastomer sustaining a cyclic loading with a frequency of $\omega = 314\ s^{-1}$ at the ambient temperature $T_0 = 297$ K. The heterogeneity of the temperature field is reduced by choosing a small radius $R = 5$ mm. Taking $\varepsilon_0 = 0.04$, the temperature at the center and at the lateral boundary are $T_{center} = 328$ K and $T_{bound} = 322$ K.

The values of the stability parameter Λ are also represented on the same graph. It is observed that the marginal stability criterion $\Lambda = 0$ is satisfied when the maximum of F_0 is attained.

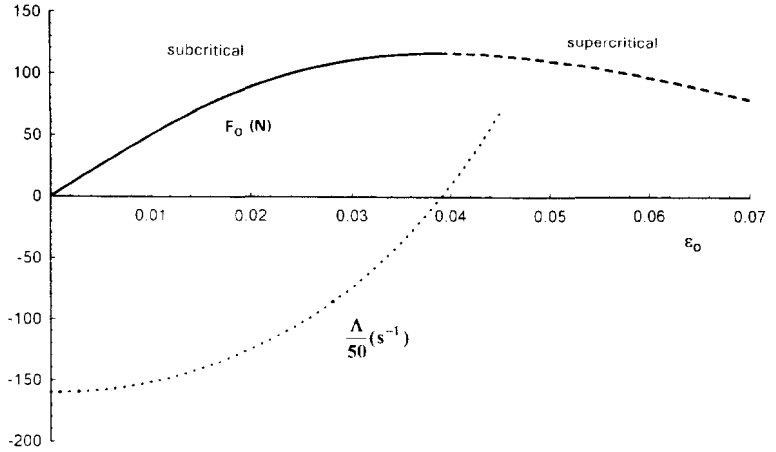

Fig. 11. Stability results for prescribed force conditions. The F_0 versus ε_0 curve represents all the possible steady states for the PEBAX elastomer at $T_0 = 297$ K and $\omega = 314\ s^{-1}$. The radius R has a value of 5 mm. The stability of these steady states depends on the boundary conditions. Λ is the stability parameter. Note the neutral stability ($\Lambda = 0$) at the maximum of the F_0–ε_0 curve, the instability of the steady states ($\Lambda > 0$) on the supercritical branch (decreasing dashed line) and the stability of the steady states ($\Lambda < 0$) on the subcritical branch (increasing continuous line).

Here again an interesting analogy can be drawn from the discussion of the stability of steady states in a thermoviscoplastic material sustaining a shear flow. Leroy and Molinari (1992) analysed the case of a material with a viscosity depending exponentially on temperature. Elasticity was neglected. When a constant velocity is applied on the boundaries, it was proved by Leroy and Molinari (1992) that all the steady states are stable, while only the steady states on the subcritical branch (the ascending branch of the stress versus velocity curve) are stable when a constant stress is applied [see also Joseph (1964, 1965)].

Leroy and Molinari (1992) also discussed the case where a mixed boundary condition, i.e. a linear combination of stress and velocity, is applied. In that case a "window" of instability can appear. The steady states are unstable when the velocity V at the boundary has a value in the window $[V-, V+]$ where $V-$ and $V+$ are critical velocities corresponding to the marginal stability criterion $\Lambda = 0$.

Mixed boundary conditions could be written for the problem analysed in the present paper as follows:

$$(\varepsilon_0 - \tilde{\varepsilon}) - \phi(F_0 - \tilde{F}) = 0 \tag{57}$$

where $\tilde{\varepsilon}$, $\tilde{F}$ and $\phi \leqslant 0$ are constants that characterize the loading conditions. The limiting cases $\phi = 0$ and $\phi = -\infty$ correspond to a prescribed displacement or force respectively. The stability condition associated to the mixed boundary condition (57) is:

$$\Lambda = \tfrac{3}{2}\omega F_0 (G'^2 + G''^2)^{-1} \left[- \frac{2\phi(\phi\tilde{F} - \tilde{\varepsilon})G''}{(1 - \phi 3\pi R^2 \sqrt{G'^2 + G''^2})^2} \left(G' \frac{dG'}{dT} + G'' \frac{dG''}{dT} \right) + \frac{dG''}{dT} \frac{F_0}{(3\pi R^2)^2} \right] - \kappa < 0. \tag{58}$$

For $\phi = -10^{-3}$, Fig. 12 shows that the steady state corresponding to marginal stability is now on the descending branch of the F_0 versus ε_0 curve. When the value of ϕ tends to zero the range of stable steady states increases. For a value of $\phi = 0$, corresponding to a prescribed axial displacement, the condition (54) is retrieved, and all the steady states are stable for the PEBAX elastomer.

Note that Leroy and Molinari (1992) have taken into account the nonuniformity of the temperature field in their stability analysis. Their results are similar to the results of the present simplified analysis where the temperature distribution has been disregarded. In view

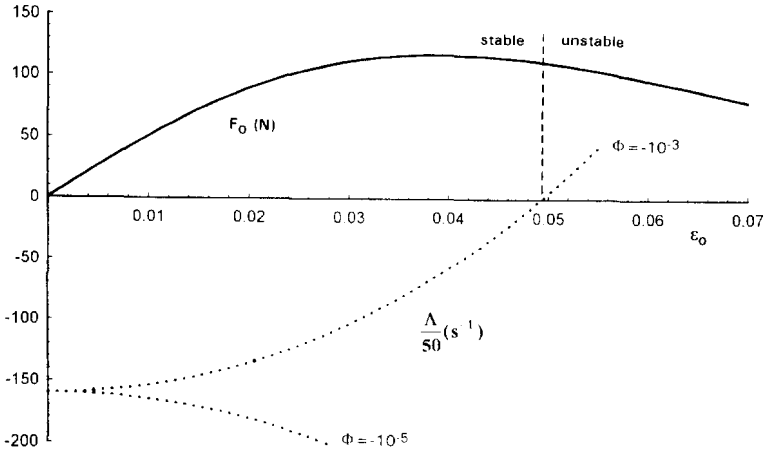

Fig. 12. Stability results for a mixed boundary condition ($-\varkappa < \phi < 0$). Note that the steady state corresponding to neutral stability ($\Lambda = 0$) is now on the supercritical (decreasing) branch.

of this similarity, the present stability results are thought to be still valid when a larger radius induces a moderate nonuniformity in the temperature field. This will be confirmed by the experimental results presented later.

6. EXPERIMENTS

6.1. *Experimental device*

The experiments were conducted at room temperature (24°C), at a frequency of $\omega/2\pi = 50\ s^{-1}$. The specimens were cylindrical with a length of $h = 30$ mm and a radius of 15 mm. The material is the PEBAX thermoplastic elastomer, having the material characteristics given in Table 1.

The MTS 1000 device, from Mechanical Testing System Co, has been used in these experiments. Dynamic testing was performed under prescribed cyclic displacement or prescribed cyclic force as described by eqns (6) and (8). When a steady state was reached, the amplitudes of the force F_0 and of the strain ε_0 defined in eqns (12) and (8) were reported in a force versus strain diagram. Several points in this diagram, representative of all the steady states reached in the experiments, are then obtained, see Fig. 13. The temperature was also measured at the center of the specimen with a transducer placed within the material through

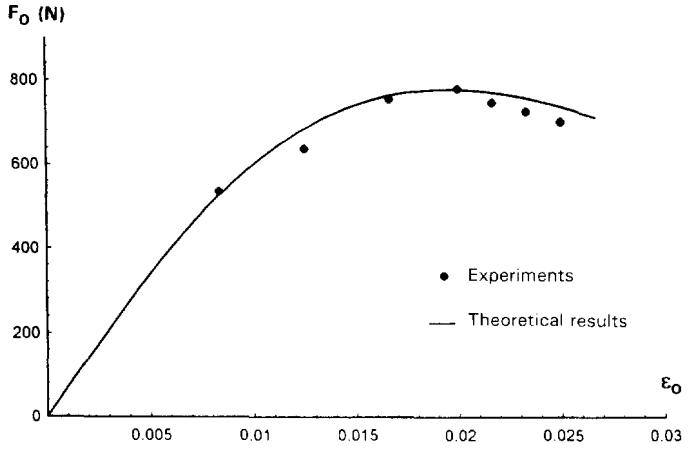

Fig. 13. Force versus deformation diagram. Large dots represent stable steady states obtained from experimental tests where the displacements were prescribed. Experiments were conducted under the following conditions: $\omega/2\pi = 50\ s^{-1}$ and $T_0 = 297$ K and the specimen radius had a value of 15 mm. Note that these results agree with the theoretical analysis (continuous line) especially for the prediction of a maximum bearing capacity.

Table 3

(a) Prescribed displacement					
Experimental conditions				Results	
W_0 (mm)	ε_0	$-F_m(N)$	$T_{init}(K)$	$F_0(N)$	T_{center}
0	0	0	297	0	297
0.25	0.0083	800	297	535	318
0.375	0.0125	800	297	637	337
0.5	0.0167	800	297	755	365
0.6	0.0200	800	297	780	398
0.65	0.0217	800	297	747	418
B 0.7	0.0233	750	373	726	423
0.75	0.0250	730	383	701	433

(b) Prescribed load					
Experimental conditions				Results	
$F_0(N)$	$-F_m(N)$	$T_{init}(K)$	W_0 (mm)	ε_0	T_{center}
A 700	700	297	0.45	0.015	80
700	700	390	0.45	0.015	80
726	726	413	destruction		
800	800	297	destruction		

a narrow channel. The temperature rise throughout the test was continuously monitored on a recorder.

The compression set-up was made of two ceramic plates that insure thermal insulation, Fig. 1. To reduce friction on these interfaces, a graphite grease was used. The heat transfer coefficient on lateral boundaries was measured for that elastomer at the value of $\lambda = 20$ W $m^{-2}K^{-1}$ given in Table 1.

A static loading force F_m [see eqn (8)] is enforced in order to keep the specimen under compression throughout the testing and to preserve the contact at the interfaces. The load F_m was reduced to avoid excessive creeping during the transient period that would render the measurements hardly useful. To reduce further creeping effects, the specimen was pre-heated in an oven up to a temperature that was estimated with the theory described herein. Doing so, the transient time to attain equilibrium was minimized and creep was observed to be almost negligeable.

It can be checked that the quasistatic condition $\omega \ll \sqrt{E/\rho h^2} = 1.05 \times 10^3\ s^{-1}$ is satisfied.

6.2. *Results and discussion*

A series of experiments were conducted with the *amplitude of the displacement being prescribed.* Table 3 gives the values of F_0 corresponding to prescribed deformations $\varepsilon_0 = w_0/h$. For each test, the values of the static force F_m and of the initial temperature (sometimes obtained by pre-heating) were reported. When a steady state was reached, the final equilibrium temperature at the center of the specimen was also reported.

The strain ε_0 was increased up to the value of $\varepsilon_0 = 0.025$. This is approximately the limit beyond which melting of the material occurs. For this strain corresponding to a displacement of $w_0 = 0.75$ mm, the temperature at the center of the cylinder was measured at the value of $T = 433$ K, very close to the melting temperature $T_{melt} = 445$ K. The temperature measured at the center of the specimen is reported in Fig. 14 for different values of the prescribed strain ε_0. For comparison we have shown on the same diagram the theoretical predictions which are close to the experimental results.

Looking again at Fig. 13, good agreement can be noted between the analytical and experimental results. Especially, a close prediction of the maximum bearing capacity is found at the value of $F_0 = 780$ N corresponding to the strain $\varepsilon_0 = 0.02$ ($w_0 = 0.6$ mm). The data used in the calculations are given in the column on the right of Table 1. These data correspond to the steady-state temperatures reached in the specimen for experiments conducted at room temperature. It is verified that $T_{red} \geqslant 314$ K in the specimen for

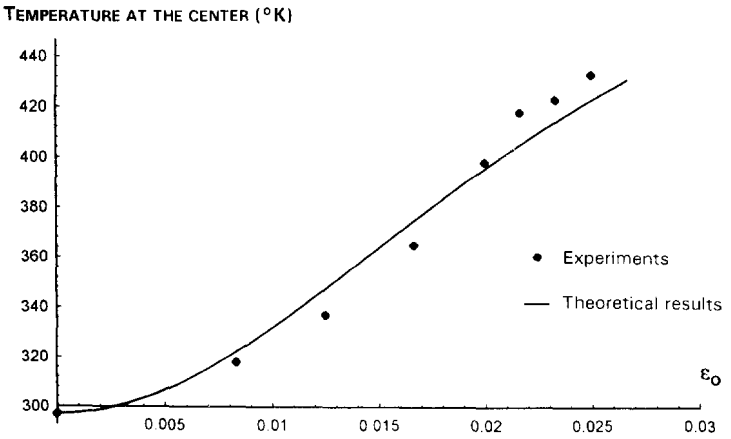

Fig. 14. Equilibrium temperatures measured at the center of the specimen (large dots) and corresponding to the steady states of the Fig. 13. These temperatures are compared with the analytical results (continuous line).

$\varepsilon_0 \geqslant 0.008$. Note the differences with the results of Fig. 9 where the following values were used: $\omega = 100\ s^{-1}$ and $T_0 = 253$ K.

All the steady states of the subcritical and on the supercritical branches have been reached for prescribed displacement w_0 smaller than 0.75 mm (melting limit). Therefore these equilibrium states are stable as predicted by the simplified linearized stability analysis.

The theoretical results were shown to be quite different in the case of *prescribed force conditions*. The theory predicts a maximum bearing capacity of $F_0 \approx 780$ N. Indeed, a test conducted at a value of $F_0 = 800$ N confirmed that no equilibrium could be reached, see Table 3(b). A continuous increase of the temperature (thermal runaway) and of the strain was observed.

For an applied value of F_0 smaller than the maximum bearing capacity, the model predicts the existence of two steady states where the one located on the subcritical branch is stable. The other one, located on the supercritical branch is unstable.

The experimental results are reported in Table 3(b). A force F_0 of 700 N was prescribed and two initial temperatures were considered, $T_{init1} = 390$ K and $T_{init2} = 297$ K. Depending on the value of the initial temperature, two paths are followed towards the steady state A, emanating from A_1 and A_2, respectively, Fig. 15. State A, acting as an attractor, is found to be the stable limiting point of these evolutions. More generally, all the subcritical steady states could be obtained under a prescribed load condition. These experimental results

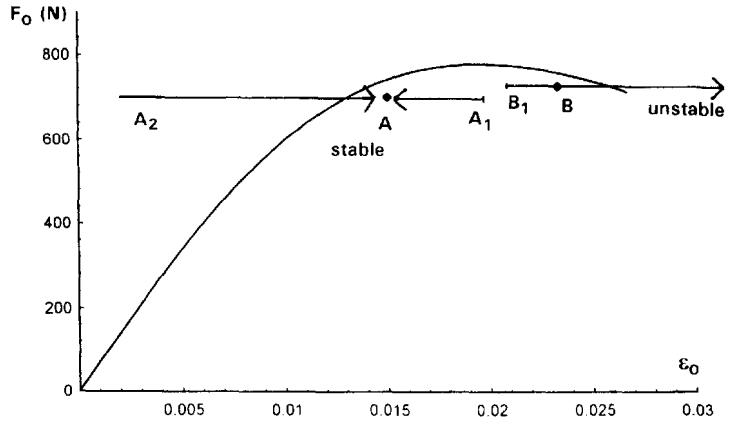

Fig. 15. Experimental results under prescribed load conditions. The arrows represent the paths followed during the tests. The stable subcritical steady-state A acts as an attractor. On the contrary the supercritical steady-state B cannot be reached. The path emanating from the initial state B_1 evolves to a thermal runaway resulting finally in the collapse of the specimen.

agree with the theoretical analysis that predicts the stability of the steady states on the subcritical branch.

On the other hand, it was not possible to reach the supercritical steady states under a prescribed load condition. Let us consider an initial temperature T_{init} of 413 K and an applied force F_0 of 726 N. The arrow starting from the initial state B_1, Fig. 15, indicates that the strain increases. But no equilibrium could be found. A thermal runaway and a collapse of the specimen was observed [see Table 3(b)]. Note that B, see Fig. 15, represents a stable steady state obtained under a prescribed displacement condition ($w_0 = 0.7$ mm, $\varepsilon_0 = 0.0233$). The amplitude of the force F_0 associated with B was measured at the value of 726 N. This steady state could not be attained under a prescribed value F_0 of 726 N. Decreasing slightly the initial temperature, the evolution path would tend to the attractor A.

7. CONCLUSION

The conditions of existence and stability of steady states have been examined for a thermoplastic elastomer under compressive cyclic loading. Small deformations and quasi-static conditions were considered. A linear isotropic viscoelastic incompressible behavior was assumed. The material response was described by a Boltzmann law with a temperature dependent relaxation function. The steady-state distributions of stresses and temperature were calculated analytically for a thermorheologically simple material whose relaxation function depends linearly on the temperature.

The stability of the steady states was shown to be conditional on the boundary conditions, except for the subcritical steady states (located on the increasing branch of the F_0–ε_0 diagram). The supercritical steady states (decreasing branch) are unstable under prescribed force conditions and stable under prescribed displacement conditions. When mixed boundary conditions are considered, the supercritical branch can be divided into stable and unstable regions.

These results are similar to those of Leroy and Molinari (1992) concerning the stability of the shear flow of a thermo–viscoplastic material. The physical content is however quite different. Elasticity was disregarded and monotonous loading conditions were considered in the work of Leroy and Molinari (1992), while here elasticity has an important role, and cyclic boundary conditions are applied.

The analytical solutions provided here are of interest for the understanding of the conditions of thermal runaway observed in the experiments. The whole set of steady states predicted by the theoretical analysis was reached experimentally by performing tests where the amplitude of the displacement was prescribed. On the contrary under prescribed load tests, only the subcritical steady states were obtained. The other steady states were shown to have no physical existence. The theoretical results are consistent with these observations.

The results obtained here, provide general trends that can be helpful in guiding the analysis and design of thermoplastic structural elements sustaining a cyclic loading.

Acknowledgments—We would like to thank P. Kerelo and A. Hildenbrand for their contribution to the experimental program. We are grateful to J. M. Rossignol and P. Dang for helpful discussions.

REFERENCES

Bai, Y. L. (1982). Thermoplastic instability in simple shear. *J. Mech. Phys. Solids* **30**, 195–207.
Christensen, R. M. (1971). *Theory of Viscoelasticity: An Introduction*. Academic Press.
Clifton, R. J. (1978). Report to the NRC Committee on material response to ultra-high loading rates.
Constable, I., Williams, J. G. and Burns, D. J. (1970). Fatigue and cyclic thermal softening of thermoplastics. *J. Mech. Engng Sci.* **12**, 20–29.
Culver, R. S. (1973). *Metallurgical Effects at High Strain Rates*, (Edited by Rohde, R. W.), pp. 519–530. Plenum Press, New York.
Ferry, J. D. (1980). *Viscoelastic Properties of Polymers*. John Wiley.
Hertzberg, R. W. (1976). *Deformation and Fracture Mechanics of Engineering Materials*. John Wiley.
Joseph, D. D. (1964). Variable viscosity effects on the flow and stability of flow in channels and pipes. *Phys. Fluids* **7**, 1761–1771.

Joseph, D. D. (1965). Non-linear heat generation and stability of the temperature distribution in conducting solids. *Int. J. Heat Mass Transfer* **8,** 281–288.
Leroy, Y. M. and Molinari, A. (1992). Stability of steady states in shear zones. *J. Mech. Phys. Solids* **40,** 181–212.
Molinari, A. (1985). Instabilité thermoviscoplastique en cisaillement simple. *J. Theor. Appl. Mech.* **4,** 659–670.
Molinari, A. and Clifton, R. J. (1987). Analytical characterization of shear localization in thermoviscoplastic materials. *J. Appl. Mech.* **54,** 806–812.
Ratner, S. B. and Korobov V. I. (1965). Self heating of plastics during cyclic deformation. *Mekh. Polymerov* **1,** 63–67.
Riddell, M. N., Koo, G. P. and O'Toole, J. L. (1966). Fatigue mechanisms of thermoplastics. *Polym. Engng Sci.* **6,** 363–370.
Takahara, A., Yamada, K., Kajiyama, T. and Takayanagi, M. (1980). Evaluation of fatigue lifetime and elucidation of fatigue in Plasticized poly(vinyl chloride) in terms of dynamic viscoelasticity. *J. Appl. Polym. Sci.* **25,** 597–614.
Takahara, A., Yamada, K., Kajiyama, T. and Takayanagi, M. (1981). Analysis of fatigue behavior of high-density polyethylene based on dynamic viscoelastic measurements during the fatigue process. *J. Appl. Polym. Sci.* **26,** 1085–1104.
Tresca, H. (1878). Flow of solids, application in forging. *Proc. Inst. Mech. Eng.* **30,** 301–327.

APPENDIX A

Effect of thermal expansion

We are aimed at analysing the influence of thermal expansion on the steady-state solutions. Taking account of the volumic dilatation induced by thermal expansion modifies the right-hand side of eqn (15):

$$\frac{\partial u}{\partial r}+\frac{u}{r}+A_1=3\alpha(T-T_0) \tag{A1}$$

where α is the thermal expansion coefficient, assumed constant.

The steady-state displacement and temperature u and T can be decomposed into a time independant part $\bar{u}$ and $\bar{T}$ (given by time averaging on a cycle) and a fluctuating part $\tilde{u}$, $\tilde{T}$. Equation (A_1) can be split into:

$$\frac{\mathrm{d}\bar{u}(r)}{\mathrm{d}r}+\frac{\bar{u}(r)}{r}+\bar{A}_1=3\alpha(\bar{T}(r)-T_0) \tag{A2}$$

$$\frac{\mathrm{d}\tilde{u}(r,t)}{\mathrm{d}r}+\frac{\tilde{u}(r,t)}{r}+\tilde{A}_1(t)=3\alpha\tilde{T}(r,t) \tag{A3}$$

where $\bar{T}(r)$ is given by eqn (40).

Let us first derive a rough estimation of the contribution of the term $3\alpha\tilde{T}$ in eqn (A_3). An estimation of the temperature variation during a cycle is obtained in Appendix B: $\Delta T=\Delta Q/\rho c$. An overestimation of the relative error induced on the dissipated energy ΔQ per cycle, by neglecting thermal expansion, will be: $\delta=\varepsilon_0 E\,\Delta\varepsilon/\Delta Q$ where E is the Young modulus and $\Delta\varepsilon=\alpha\Delta T$ is the linear thermal expansion. For the PEBAX elastomer we have $\alpha=10^{-5}\ \mathrm{K}^{-1}$, $E=150$ MPa. Thus the relative error $\delta=\varepsilon_0 E\alpha/\rho c=0.00075\,\varepsilon_0$ is quite small, and the term $3\alpha\tilde{T}$ can be dropped in eqn (A_3).

Therefore, it can be shown that the thermal expansion coefficient has a negligeable influence on the steady-state solutions. However, it modifies the value of the static part of the axial force when the axial displacement is controlled.

APPENDIX B

Evaluation of the temperature fluctuation over a cycle

With the assumption that the process is adiabatic ($k=0$, $\lambda=0$), an upper bound of the temperature fluctuation, over a cycle, is calculated by integrating the heat equation (4):

$$\Delta T=\frac{\Delta Q}{\rho c}=\frac{3\pi\varepsilon_0^2 G''}{\rho c}.$$

Typical values for a PEBAX elastomer at $T_0=293$ K are: $G''=8$ MPa, $\rho c=2\times10^6\ \mathrm{J\ K^{-1}\ m^{-3}}$. For $\varepsilon_0=0.05$, an upper value of the amplitude of the deformation prescribed in the experiments, the temperature fluctuation $\Delta T=0.094$ K is small enough to justify the approximation (19).

APPENDIX C

Simplified analysis for an uniform temperature field

Considering a slender specimen ($R/h\ll1$) or a material with a large thermal conductivity, the distribution of temperature is nearly uniform. The energy eqn (4) reads:

$$\rho c\frac{\partial T}{\partial t}-\frac{k}{r}\frac{\partial}{\partial r}\left(r\frac{\partial T}{\partial r}\right)=\dot{Q}. \tag{C1}$$

Let us define the mean value of T in a cross-section by:

$$\langle T\rangle = \frac{1}{\pi R^2}\int_0^R T(r)2\pi r\,\mathrm{d}r. \tag{C2}$$

From eqn (C1), we obtain the relation:

$$\rho c\frac{\mathrm{d}}{\mathrm{d}t}\langle T\rangle - k\frac{2}{R^2}\int_0^R \frac{\partial}{\partial r}\left(r\frac{\partial T}{\partial r}\right)\mathrm{d}r = \langle \dot{Q}\rangle$$

that, after using eqn (9), leads to:

$$\rho c\frac{\mathrm{d}}{\mathrm{d}t}\langle T\rangle + \frac{2}{R}\lambda[T(R) - T_0] = \langle \dot{Q}\rangle. \tag{C3}$$

When the radius R decreases to zero, the relative difference of temperature from the center to the boundary

$$\delta_1 = \frac{T_{|r=0} - T_{|r=R}}{T_{|r=0}}$$

tends to zero. [For example, considering the particular case of the steady-state temperature distribution given by eqn (43), it can be checked that: $\delta_1 = 0\ (R^2)$.]

Then the temperature can be considered as constant in a cross-section and eqn (C3) can be rewritten as:

$$\rho c\frac{\mathrm{d}T}{\mathrm{d}t} + \kappa(T - T_0) = \dot{Q} \tag{C4}$$

with $\kappa = 2\lambda/R$.

Considering now a steady-state solution, eqn (C4) reads after time averaging on a cycle:

$$\kappa(T_m - T_0) = \frac{\omega}{2\pi}\Delta Q = \tfrac{3}{2}\omega\varepsilon_0^2 G''(\omega, T_m). \tag{C5}$$

Moreover, eqns (31) and (34) reduce to:

$$F_0 = \sigma_0\pi R^2 = 3\pi\varepsilon_0 R^2 G'(\omega, T_m)\sqrt{1 + (\tan\psi)^2} \tag{C6}$$

where the axial stress $\sigma_0 = \sigma_{zz}$ is now uniform, and $\tan\psi = G''(\omega, T_m)/G'(\omega, T_m)$. The system of eqns (C5) and (C6) provides T_m and $\varepsilon_0 = w_0/h$ in terms of F_0.